FEBS Letters

FEBS PRESS science publishing by scientists

Visualizing the movement of the amphipathic helix in the respiratory complex I using a nitrile infrared probe and SEIRAS

Ana Filipa Santos Seica[1], Johannes Schimpf[2], Thorsten Friedrich[2] and Petra Hellwig[1,3]

1 Laboratoire de Bioélectrochimie et Spectroscopie, UMR 7140, CMC, Université de Strasbourg CNRS, France
2 Institut für Biochemie, Albert-Ludwigs-Universität Freiburg, Germany
3 University of Strasbourg Institute for Advanced Studies (USIAS), France

Correspondence
P. Hellwig, Laboratoire de Bioélectrochimie et Spectroscopie, UMR 7140, CMC, Université de Strasbourg, CNRS, 4 Rue Blaise Pascal, Strasbourg 67081, France
Tel: +33 368 851273
E-mail: hellwig@unistra.fr

(Received 30 August 2019, revised 20 September 2019, accepted 23 September 2019, available online 7 October 2019)

doi:10.1002/1873-3468.13620

Edited by Peter Brzezinski

Conformational movements play an important role in enzyme catalysis. Respiratory complex I, an L-shaped enzyme, connects electron transfer from NADH to ubiquinone in its peripheral arm with proton translocation through its membrane arm by a coupling mechanism still under debate. The amphipathic helix across the membrane arm represents a unique structural feature. Here, we demonstrate a new way to study conformational changes by introducing a small and highly flexible nitrile infrared (IR) label to this helix to visualize movement with surface-enhanced IR absorption spectroscopy. We find that labeled residues K551C^{L} and Y590C^{L} move to a more hydrophobic environment upon NADH reduction of the enzyme, likely as a response to the reorganization of the antiporter-like subunits in the membrane arm.

Keywords: infrared nitrile labels; respiratory complex I; SEIRAS

The NADH ubiquinone oxidoreductase, most commonly known as respiratory complex I, is a large membrane-bound enzyme that contributes to the electrochemical potential by coupling electron transfer from NADH to ubiquinone with translocation of four protons across the membrane, vital for the synthesis of ATP and the exchange of solutes and nutrients across the membrane and for motility [1].

Complex I has an L-shaped structure first seen by negative stain electron microscopy [2,3], with a membrane arm and a peripheral arm that extends at an angle of ~ 120° into the aqueous medium. The peripheral arm contains all the prosthetic groups, including one flavin mononucleotide (FMN) and 8–10 iron–sulfur (Fe-S) clusters, as well as the NADH binding site [4].

Oxidation of NADH is catalyzed at the FMN binding site at the distal end of the peripheral arm, while the reduction of ubiquinone occurs at cluster N2 close to the intersection of the two arms [5–7]. Proton translocation takes place in the membrane arm, and the coupling of this process to electron transfer is still under debate. The structural arrangement of the membrane arm of the complex has been visualized at low resolution by cryo-electron microscopy [8] and at higher resolution by X-ray diffraction [9–11]. Bacterial complex I is constituted by 13–16 subunits adding to a molecular mass of ~ 550 kDa. Generally, the subunits are named NuoA to NuoN. NuoL, M, and N are involved in proton translocation and are homologous to subunits of monovalent cation/proton antiporters [12,13] (Fig. 1A). Each of NuoL, M, and N contains 14 transmembrane (TM) helices [13]. It was proposed that quinone reduction induces concerted long-range conformational changes in the antiporter-like subunits controlling proton translocation [14]. NuoL is located

Abbreviations
FMN, flavin mononucleotide; IR, infrared; KSCN, potassium thiocyanate; Ni-NTA, nickel–nitrilotriacetic acid; SEIRAS, surface-enhanced IR absorption spectroscopy; TM, transmembrane.

at the distal end of the membrane arm with a C-terminal domain that extends to a unique 110 Å long amphipathic helix parallel to the membrane [15]. The horizontal helix is located between TM helix 15 and TM helix 16 of NuoL and was first revealed by crystallographic analysis by Efremov *et al*. in 2010 [9]. The attractive hypothesis that electron transfer induces a piston-like movement of the horizontal helix to open and close proton pathways in NuoL, M, and N was refuted by mutagenesis studies indicating that the helix acts more like a clamp to tighten the structure of the membrane arm [16–18]. Zhu and Vik [19] proposed that the horizontal helix might transmit conformational changes opening the quinone binding site.

The movement of the helix was probed with fluorescence and nitroxide labels. Slight conformational changes of the helix during the reduction of the complex by NADH became evident but not a large rearrangement [20]. However, it is possible that the size of the fluorophore and the nitroxide label influenced the conformational flexibility of the helix. In order to address this question, we used a smaller probe the SCN group that can be detected by means of infrared (IR) spectroscopy. Nitrile- and thiocyanate-derivatized amino acids are particularly attractive IR probes due to their smaller size and the frequency of the stretching mode being in a relatively clear region of the IR spectrum ($\nu C{\equiv}N \sim 2100–2240\ cm^{-1}$) [21,22].

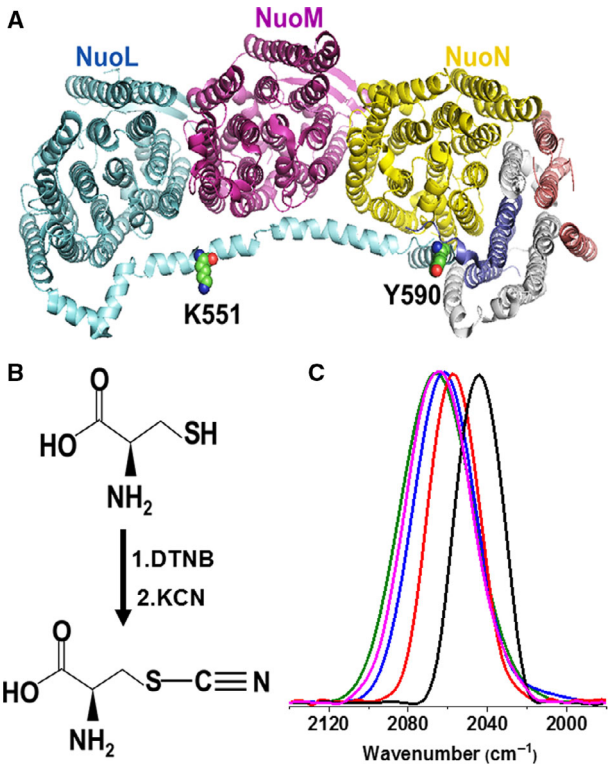

Fig. 1. (A) Structure of the membrane arm of *Escherichia coli* complex I and the positions of the residues under investigation (PDB: 3RKO), (B) cysteine cyanylation protocol, and (C) absorbance spectrum of potassium thiocyanate dissolved in THF (2044 cm^{-1}; black), DMSO (2057 cm^{-1}; red), ethanol (2061 cm^{-1}; blue), MOPS buffer pH 7.0 (2064 cm^{-1}; pink), and methanol (2066 cm^{-1}; green).

The thiocyanate moiety is generated by chemical modification of the free thiol of an accessible cysteine residue and can thus be inserted at any cysteine site either being a natural residue or resulting from mutagenesis [23]. Previous studies on the influence of the microenvironment on the signature of the $SC{\equiv}N$ stretching frequency in proteins showed typical signals at about 2160 cm^{-1} for labeled ribonuclease S [24] and for the protein calmodulin [25].

In the IR spectrum, the CN stretching frequency is a balance of two different types of hydrogen-bonding interactions, σ-H-bonding and π-H-bonding water molecules. Cho and coworkers [26] discovered that the $C{\equiv}N$ stretching frequency of cyanomethane (CH_3CN) is determined by the water molecules surrounding the $C{\equiv}N$ group. The bond of the water molecule (σ-bonding with nitrogen lone pair) will result in a blueshift, whereas interactions of water molecules with the π-orbital of the nitrile moiety (termed π-bonding) will lead to a redshift. Also, the hydrophobicity of the environment will influence the signature. In a study using the label bound to POPC phospholipid bilayers, for example, a more hydrophobic environment induced a shift of 6 cm^{-1} [27]. Another factor that is discussed for the interpretation of the potential shifts is the electric field. It is noted, however, that in contrast to the well-known effects on carbonyl stretching vibrations, the effect on the CN frequency is rather weak, due to their ability to accept hydrogen bonds [28,29].

In this work, we labeled respiratory complex I with SCN residues and studied the changes of the probe *in situ* by the addition of NADH. The variants studied were selected on the basis of the structural studies previously reported [20] with the aim to further investigate changes in the membrane after reduction of the enzyme with NADH. Our approach included the use of surface-enhanced IR absorption spectroscopy (SEIRAS) giving access to the data by using just a monolayer of protein and therefore only a very small amount of protein in the micromolar range [30].

Materials and methods

Sample preparation

Complex I was prepared as previously described in Steimle *et al*. [18]. Variants with cysteine mutations at positions

$K551^L$ and $Y590^L$ (Fig. 1A) in the amphipathic helix of the membrane arm were generated as described in [20]. Protein samples were purified and stored in 50 mM MES/NaOH, 50 mM NaCl, 5 mM $MgCl_2$, and 0.005% MNG-3, pH 6.0.

Cyanide labeling of complex I and the $K551C^L$ and $Y590C^L$ variants

The strategy for converting the thiol group of the cysteine residue (PSH) into thiocyanates was adapted from Fafarman *et al.* (Fig. 1B) [23]. The protein reacts with 5,5′-dithiobis-(2-nitrobenzoic acid) (DTNB or Ellman's reagent) to form the mixed protein–thionitrobenzoic acid disulfide (PS-TNB), followed by displacement by cyanide (CN^-), to form the protein–thiocyanate (PS-CN) [24].

Ten micromolar complex I and the variants were incubated at 4 °C with dithiothreitol (DTT) for 30 min to reduce the cysteine residues, followed by removal of excess DTT with two consecutive Sephadex G50 columns. The protein was incubated at 4 °C with a 44-fold molar excess of DTNB for 1 h, and excess DTNB was also removed by two consecutive Sephadex G50 runs. Finally, 6 mM potassium cyanide (KCN) was added to the protein solution. The spectrum of complex I treated with this procedure did not show any significant thiocyanate signature, demonstrating that the wild-type complex contains no accessible cysteine residues (Fig. S1A).

Potassium thiocyanate solutions

A solution of 30 mM potassium thiocyanate (KSCN) was prepared in the following solvents, respectively: DMSO, THF, ethanol, methanol, and MES buffer pH 6.0. The spectra were normalized to the same intensity.

IR spectroscopy

A configuration allowing the acquisition of FTIR spectra in the ATR mode was employed, including a silicon crystal with a 3 mm surface diameter as a single reflection ATR unit. IR spectra were measured on a Vertex 70 FTIR spectrometer from Bruker, Karlsruhe, Germany (Globar source, KBr Beamsplitter, mercury cadmium telluride detector) with 40-kHz scanner velocity, 256 scans, and 4 cm^{-1} resolution. Typically, 12 spectra were averaged. A baseline correction was performed.

Surface-enhanced FTIR spectroscopies

A nickel–nitrilotriacetic acid (Ni-NTA) self-assembled monolayer was adapted from techniques reported before [30–33]. First, a gold layer was formed on the Si crystal. The plating solution is a 1 : 1 : 1 mix (vol/vol/vol) of (A) 15 mM $NaAuCl_4$, (B) 150 mM Na_2SO_3 + 50 mM $Na_2S_2O_3$ + 50 mM NH_4Cl, and (C) 2% HF (wt/vol: 1 mL). Crystal and the plating solution were heated at 65 °C for 10 min together. The silicon prism was covered with the solution for 40 s, and deposition was stopped by washing the crystal surface with water, followed by drying the surface with a stream of argon.

The solution dithiodipropionic acid di(N-hydroxysuccinimide ester) (DTSP) in DMSO was allowed to self-assemble for 1 h. The self-assembled monolayer was immersed in *N*α,*N*α-bis(carboxymethyl)-L-lysine for 3 h and rinsed with water. Finally, the surface was incubated with $Ni(ClO_4)_2$ for 1 h. Complex I was incubated with 50 μM NADH for 4 h on ice before immobilization of the protein onto the Ni-NTA surface.

Deconvolution of the amide I signal of WT and mutants

The amide I signal of the protein was used to confirm the structural integrity of the complex after labeling and immobilization. Deconvolution was performed after calculation of the fourth derivative to estimate the number and position of the components of amide I band, followed by deconvolution using the Gaussian profile of each component.

Results

A stable monolayer of complex I immobilized through an N-terminal His-tag on NuoF to a modified gold layer was obtained as described before [30]. Figure 2A shows the absorbance spectrum of $K551C^L$ variant after reacting with DTNB and KCN to form the protein–thiocyanate. The spectrum includes characteristic signals of amide I and amide II and of the thiocyanate bond.

The amide I band of all samples studied was highly comparable, confirming that there are no detectable differences in the conformation of wild-type and mutants (Fig. S2). Due to the SEIRAS approach used, the SCN signal can be directly evidenced from the absorbance spectra in the spectral region characteristic for triple bonds, between 2200 and 2000 cm^{-1}.

The $K551C^L$ variant in the oxidized state shows a thiocyanate band at 2128 cm^{-1}. After reduction with NADH, the band is shifted to lower wavenumbers at 2123 cm^{-1} (Fig. 2B). The difference spectrum highlights the changes in the spectral signature, and the observed change of 18 cm^{-1} reveals a movement of the residue at position 551^L toward a more hydrophobic microenvironment upon reduction by NADH and thus toward the membrane. $K551^L$ is part of a regular α-helical structure, pointing away from the membrane arm toward the cytosol, at the level of the interface between NuoL and NuoM [14].

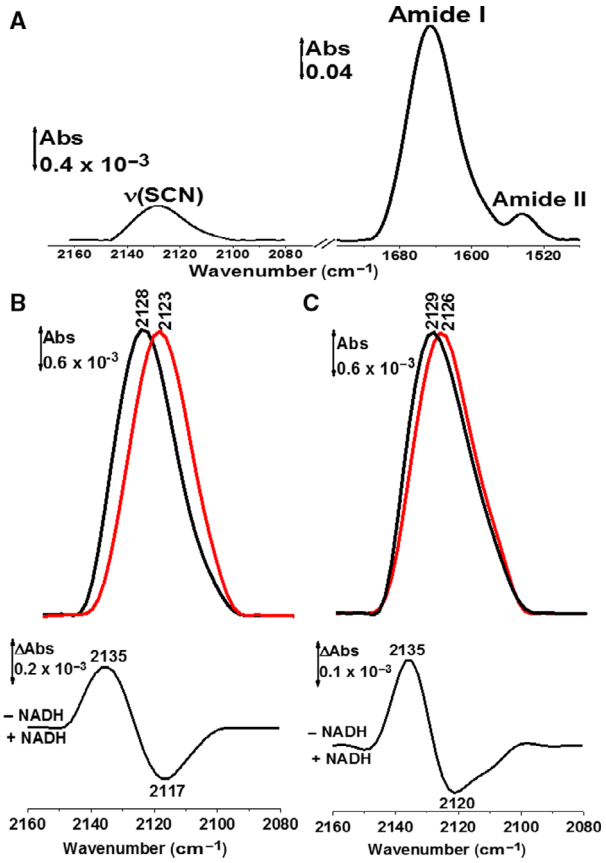

Fig. 2. (A) Absorbance spectrum of labeled complex I, spectra of the ν(SC≡N), and amide I and amide II band of *Escherichia coli* complex I K551C^{L} immobilized onto a Ni-NTA SAM. The intensity of the ν(SC≡N) band was increased for better visibility. (B) Spectra of ν(SC≡N) of labeled K551C^{L} and (C) Y590C^{L} incubated with (red line) and without (black line) NADH and the difference spectra after normalization of the thiocyanate band.

The second residue in variant Y590C^{L} is found at the end of the amphipathic helix close to the hinge leading to the most C-terminal TM helix 16. It is located in close proximity to NuoN at the interface between the membrane bilayer and the cytosol [14]. Figure 2C shows the νSCN signal of the label at 2129 cm^{-1} in the oxidized state of the variant, and after reduction by NADH, the thiocyanate band is shifted to lower wavenumbers as observed with the K551C^{L} variant. The difference spectra highlight a change of 15 cm^{-1} for the mutation at position 590^{L}, a little smaller compared to that of position 551 (Fig. 2C). However, both samples point toward a slight movement of the helix after treatment with NADH, indicating that these positions of the helix turn toward the hydrophobic phase of the membrane arm.

Discussion

The placement of nitrile labels to cysteine residues of *Escherichia coli* respiratory complex I allowed to monitor minor movements of the amphipathic horizontal helix of NuoL in the membrane arm upon reduction by NADH. When subtracting the spectra before and after addition of NADH, differences of 15–18 cm^{-1} for the signals of the label visualize experimentally a reorganization of distinct positions within the helix toward a more hydrophobic environment. Previous EPR and fluorescence spectroscopy studies by Steimle *et al*. [20] pointed to a nearly imperceptible movement of the helix upon reduction by NADH.

Even if the studied residues are pointing away from the protein in the oxidized state, the reduction may induce a change in position, which would be hindered by a too large label. So, in contrast to these studies, the nitrile label will show a higher sensitivity to the conformational changes due to the smaller size of the label.

The effect of the environment on the vibrational mode of KSCN, including hydrogen bonding and polarizability, can be seen from the data obtained in different solvents (Fig. 1C). When bound to a cysteine residue, the SCN vibrational mode upshifts and the broadness or more specifically the FWHM (full width at half maximum) changes. The study in different solvents helps to evaluate the effect of a more or less hydrophilic environment on the probe, when comparing, for example, two states of a protein during a reaction [34].

The significance of the shifts is derived from comparison to similar experiments on other proteins. Indeed, shifts below 5 cm^{-1} have been found to be relevant [27]. Tucker *et al*. studied the membrane-binding amphipathic peptide, mastoparan x (MPx peptide) by infrared spectroscopy using a PheCN probe. The peptide MPx-CNy in water showed a CN stretching vibration at 2235 cm^{-1}. When bound to POPC phospholipid bilayers, the CN stretching vibration shifted by 6–2229 cm^{-1} indicating a more hydrophobic and less solvent accessible environment for the CN probe [27]. A change of the hydrogen-bonding environment, or the presence or absence of water molecules after addition of NADH, may also influence the spectral signature. As described in the introduction, the red-shift can also be attributed to a weaker interaction of the hydrogen bonds with the σ-bonding with nitrogen lone pair [28].

Conclusion

So, the shifts observed here correspond to a movement toward a significantly more hydrophobic environment

or an environment with weaker hydrogen bonds upon NADH addition. It was proposed that the enzyme cycles between an 'open' conformation (NADH-reduced state) and a 'closed' conformation (oxidized state) [35]. The three antiporter-like subunits NuoL, M, and N are involved in proton translocation most likely driven by a rearrangement of the hydrophilic loops and the position of TM helices within the membrane. Mamedova *et al*. [35] predicted that upon NADH binding, the peripheral arm of the complex adopts a more open conformation, with increased distances between subunits, and single-particle analysis showed that the membrane domain also expands. The most likely explanation of our observation is that the movement of the positions on the amphipathic helix is an indirect effect that results from a structural compensation of the movement of the membrane arm during reduction [36] that would be in line with the conformational change suggested above to occur after NADH addition.

Acknowledgements

AFSC and PH are grateful to the IDEX International doctoral program (PDI) from the University of Strasbourg. JS and TF were supported by the Deutsche Forschungsgemeinschaft (DFG) by grant 278002225/RTG 2202.

Author contributions

AFSS prepared the labeled samples and measured the IR spectra; JS prepared the mutant enzymes; TF analyzed the data; PH planned the experiments and analyzed the data. All authors contributed to the manuscript preparation.

References

1 Berrisford JM, Baradaran R and Sazanov LA (2016) Structure of bacterial respiratory complex. *Biochim Biophys Acta Bioenerg* **1857**, 892–901.
2 Guénebaut V, Vincentelli R, Mills D, Weiss H and Leonard KR (1997) Three-dimensional structure of NADH dehydrogenase from *Neurospora crassa* by electron microscopy and conical tilt reconstruction. *J Mol Biol* **265**, 409–418.
3 Leonard K, Haiker H and Weiss H (1987) Three-dimensional structure of NADH: ubiquinone reductase (complex I) from *Neurospora* mitochondria determined by electron microscopy of membrane crystals. *J Mol Biol* **194**, 277–286.
4 Pohl T, Bauer T, Dörner K, Stolpe S, Sell P, Zocher G and Friedrich T (2007) Iron-sulfur cluster N7 of the NADH:ubiquinone oxidoreductase (complex I) is essential for stability but not involved in electron transfer. *Biochemistry* **46**, 6588–6596.
5 Brandt U (2006) Energy converting NADH:quinone oxidoreductase (complex I). *Annu Rev Biochem* **75**, 69–92.
6 Carroll J, Fearnley IM, Skehel JM, Shannon RJ, Hirst J and Walker JE (2006) Bovine complex I is a complex of 45 different subunits. *J Biol Chem* **281**, 32724–32727.
7 Grigorieff N (1998) Three-dimensional structure of bovine NADH:ubiquinone oxidoreductase (complex I) at 22 A° in ice. *J Mol Biol* **277**, 1033–1046.
8 Baranova EA, Holt PJ and Sazanov LA (2007) Projection structure of the membrane domain of *Escherichia coli* respiratory complex I at 8 A° resolution. *J Mol Biol* **366**, 140–54.
9 Efremov RG, Baradaran R and Sazanov LA (2010) The architecture of respiratory complex I. *Nature* **465**, 441–445.
10 Hunte C, Zickermann V and Brandt U (2010) Functional modules and structural basis of conformational coupling in mitochondrial complex I. *Science* **329**, 448–451.
11 Efremov RG and Sazanov LA (2011) Structure of the membrane domain of respiratory complex I. *Nature* **476**, 414–420.
12 Sazanov LA (2007) Respiratory complex I: mechanistic and structural insights provided by the crystal structure of the hydrophilic domain. *Biochemistry* **46**, 2275–2288.
13 Holt PJ, Morgan DJ and Sazanov LA (2003) The location of NuoL and NuoM subunits in the membrane domain of the *Escherichia coli* complex I: implications for the mechanism of proton pumping. *J Biol Chem* **278**, 43114–43120.
14 Baradaran R, Berrisford JM, Minhas GS and Sazanov LA (2013) Crystal structure of the entire respiratory complex I. *Nature* **494**, 441–445.
15 Ohnishi T, Nakamaru-Ogiso E and Ohnishi ST (2010) A new hypothesis on the simultaneous direct and indirect proton pump mechanisms in NADH-quinone oxidoreductase (complex I). *FEBS Lett* **584**, 4131–4137.
16 Torres-Bacete J, Sinha PK, Matsuno-Yagi A and Yagi T (2011) Structural contribution of C-terminal segments of NuoL (ND5) and NuoM (ND4) subunits of complex I from *Escherichia coli*. *J Biol Chem* **286**, 34007–34014.
17 Belevich G, Knuuti J, Verkhovsky MI, Wikström M and Verkhovskaya M (2011) Probing the mechanistic role of the long α-helix in subunit L of respiratory complex I from *Escherichia coli* by site-directed mutagenesis. *Mol Microbiol* **82**, 1086–1095.
18 Steimle S, Bajzath C, Dörner K, Schulte M, Bothe V and Friedrich T (2011) Role of subunit NuoL for proton translocation by respiratory complex I. *Biochemistry* **50**, 3386–3393.
19 Zhu S and Vik SB (2015) Constraining the lateral helix of respiratory complex I by cross-linking does not

impair enzyme activity or proton translocation. *J Biol Chem* **290**, 20761–20773.
20 Steimle S, Schnick C, Burger E-M, Nuber F, Krämer D, Dawitz H, Brander S, Matlosz B, Schäfer J, Maurer K *et al*. (2015) Cysteine scanning reveals minor local rearrangements of the horizontal helix of respiratory complex I. *Mol Microbiol* **98**, 151–161.
21 Kwang-Im O, Jun-Ho C, Joo-Hyun L, Jae-Beom H, Hochan L and Minhaeng C (2008) Nitrile and thiocyanate IR probes: molecular dynamics simulation studies. *J Chem Phys* **128**, 154504.
22 Getahun Z, Huang C-Y, Wang T, De León B, DeGrado WF and Gai F (2003) Using nitrile-derivatized amino acids as infrared probes of local environment. *J Am Chem Soc* **125**, 405–411.
23 Fafarman AT, Webb LJ, Chuang JI and Boxer SG (2006) Site-specific conversion of cysteine thiols into thiocyanate creates an IR probe for electric field in proteins. *J Am Chem Soc* **128**, 13356–13357.
24 Bagchi S, Boxer SG and Fayer MD (2012) Ribonuclease S dynamics measured using a nitrile label with 2D IR vibrational echo spectroscopy. *J Phys Chem B* **116**, 4034–4042.
25 Dalton SR, Vienneau AR, Burstein SR, Xu RJ, Linse S and Londergan CH (2018) Cyanylated cysteine reports site-specific changes at protein-protein-binding interfaces without perturbation. *Biochemistry* **57**, 3702–3712.
26 Choi J-H, Oh K-I, Lee H, Lee C and Cho M (2008) Nitrile and thiocyanate IR probes: quantum chemistry calculation studies and multivariate least-square fitting analysis. *J Chem Phys* **128**, 134506.
27 Tucker MJ, Getahun Z, Nanda V, De Grado WF and Gai F (2004) A new method for determining the local environment and orientation of individual side chains of membrane-binding peptides. *J Am Chem Soc* **126**, 5078–5079.
28 Deb P, Haldar T, Kashid SM, Banerjee S, Chakrabarty S and Bagchi S (2016) Correlating nitrile IR frequencies to local electrostatics quantifies noncovalent interactions of peptides and proteins. *J Phys Chem B* **120**, 4034–4046.
29 Slocum JD and Webb LJ (2016) Nitrile probes of electric field agree with independently measured fields in green fluorescent protein even in the presence of hydrogen bonding. *J Am Chem Soc* **138**, 6561–6570.
30 Kriegel S, Uchida T, Osawa M, Friedrich T and Hellwig P (2014) Biomimetic environment to study *E. coli* complex I through surface-enhanced IR absorption spectroscopy. *Biochemistry* **53**, 6340–6347.
31 Grytsyk N, Sugihara J, Kaback HR and Hellwig P (2016) pKa of Glu325 in LacY. *Proc Natl Acad Sci USA* **114**, 1530–1535.
32 Grytsyk N, Seiça AFS, Sugihara J, Kaback HR and Hellwig P (2019) Arg302 governs the pKa of Glu325 in LacY. *Proc Natl Acad Sci USA* **116**, 4934–4939.
33 Ataka K and Heberle J (2006) Use of surface enhanced infrared absorption spectroscopy (SEIRA) to probe the functionality of a protein monolayer. *Biopolymers* **82**, 415–419.
34 van Wilderen LJG, Kern-Michler D, Muller-Werkmeister HM and Bredenbeck J (2014) Vibrational dynamics and solvatochromism of the label SCN in various solvents and hemoglobin by time dependent IR and 2D-IR spectroscopy. *Phys Chem Chem Phys* **16**, 19643.
35 Mamedova AA, Holt PJ, Carroll J and Sazanov LA (2004) Substrate-induced conformational change in bacterial complex I. *J Biol Chem* **279**, 23830–23836.
36 Di Luca A, Mühlbauer ME, Saura P and Kaila VRI (2018) How inter-subunit contacts in the membrane domain of complex I affect proton transfer energetics. *Biochim Biophys Acta Bioenerg* **1859**, 734–741.

Supporting information

Additional supporting information may be found online in the Supporting Information section at the end of the article.

Fig. S1. Absorbance spectrum of *E. coli* complex I immobilized onto a Ni-NTA SAM of (A) wild type, (B) labeled $K551C^{L}$ and (C) labeled $Y590C^{L}$.

Fig. S2. Deconvolution of amide I band of *E. coli* complex I prepared in 50 mM MES/NaOH, 50 mM NaCl, 5 mM $MgCl_2$ and 0.005% MNG-3 (pH 6.0) immobilized onto a Ni-NTA SAM of (A) wild type, (B) labeled $K551C^{L}$ and (C) labeled $Y590C^{L}$.